Highlights:

- Two bright AIE-active photosensitizers (PSs) with alkyne group could overcome the problem of conventional aggregation caused fluorescence quenching.

- Thiol-yne click reaction was used to prepare biocompatible PS@BSA nanoparticles with better water dispersibility and small nanoscale size.

- PS@BSA nanoparticles achieved great photodynamic therapy effect for the B16-F10 cancer cells because of effective generation of $O_2^{-\cdot}$ and ·OH.

- The universal and eco-friendly method was proposed to prepare hydrophilic AIE-active PS's NPs.

Light-Triggered Click Reaction to Fabricate Bright Bovine Serum Albumin Encapsulates Photosensitizer's Nanoparticles for Effective Photodynamic Therapy of Melanoma Cells

Yifan Li[1], Yitao Fan[1], Qian Liu[2], Xuya Wang[2], Yuxia Jin[2], Muzhou Teng*[1.2]

1. Department of Dermatology, The Second Hospital & Clinical Medical School, Lanzhou University, Lanzhou, China.

2. Gansu Provincial Maternity and Child-Care Hospital (Gansu Provincial Central Hospital), Lanzhou, China.

Corresponding author: Prof. Muzhou Teng (smutmz@126.com)

Abstract

Photodynamic therapy (PDT) has emerged as a promising anticancer strategy due to its non-invasive nature and precise spatiotemporal control. However, conventional photosensitizers (PSs) suffer from aggregation-caused quenching (ACQ), poor hydrophilicity, and serious oxygen dependence, limiting their clinical utility. To address these challenges, we developed an efficient strategy to fabricate hydrophilic aggregation-induced emission (AIE)-active Bovine Serum Albumin (BSA) Encapsulates PSs via an effective light-mediated thiol-yne click reaction. By designing alkynyl-functionalized AIE-active PSs with strong

generating capability of type I/II reactive oxygen species (ROS), we achieved fast combination with thiol-rich BSA under UV light irradiation, forming stable BSA@AIE-active PSs' nanoparticles (NPs). The resulting NPs exhibited excellent water dispersibility, bright fluorescence and intense ROS generation. *In vitro* studies demonstrated their outstanding PDT effect to melanoma cell (B16-F10) under white light irradiation. This work proposed a universal, scalable, and eco-friendly platform for constructing AIE-active hydrophilic PS's NPs, overcoming longstanding hurdles in PS's hydrophobicity and fabrication complexity.

Keywords: Aggregation-induced emission, click reaction, photodynamic therapy, bovine serum albumin, melanoma cell

Introduction

Photodynamic therapy (PDT), as a non-invasive and spatiotemporally controllable treatment technology, has attracted increasing research interests in biomedical field.[1-3] By leveraging light-activated photosensitizers (PSs) to generate cytotoxic reactive oxygen species (ROS), PDT offers an effective approach to eliminate cancer cells while minimizing damage to healthy tissues.[4] However, some disadvantages of conventional PSs make them difficult to achieve highly efficient practical applications, such as typical and head-scratching aggregation-caused quenching (ACQ) effect,[5] poor water solubility, and serious oxygen

dependence.[6] These drawbacks often lead to reduced fluorescence and ROS generation efficiency, suboptimal biocompatibility, and limited therapeutic efficiency. In recent years, aggregation-induced emission (AIE)-active PSs have emerged as a revolutionary class of photosensitizers (PSs), [7-8] addressing effectively the ACQ problem by exhibiting enhanced luminescence and ROS generation in the aggregated state.[9-11] Despite their a series of advantages, the hydrophobic nature of most aromatic AIE-active PSs poses challenges in achieving stable aqueous dispersion, necessitating additional chemical modifications or carrier systems to improve biocompatibility.[12-15] This trade-off between functionality and practicality underscores the urgent need for innovative strategies to streamline the fabrication of AIE-based nanoplatforms without compromising performance.

Click chemistry, renowned for its high efficiency, selectivity, and mild reaction conditions, has become an important protocol to fabricate biomedical materials and modify surface,[16-19] which has promising applications in the fields of bioconjugation and nanomaterial engineering. Among its diverse reactions, the light-triggered thiol-yne click reaction stands out for its spatiotemporal control and catalyst-free nature, making it particularly suitable for biomedical applications.[20-23] By exploiting the rapid and specific coupling between alkyne and thiol groups under light irradiation, this strategy enables precise functionalization of biomolecules

while preserving their native activity. Building on this principle, we herein report a novel methodology for constructing hydrophilic AIE-active PSs' nanoparticles via a one-step photo-click reaction between alkynyl-functionalized AIE-active PSs and thiol group contained Bovine Serum Albumin (BSA). This approach not only circumvents the need for toxic catalysts but also integrates the advantages (aggregation enhances fluorescence and ROS efficiency) of AIE-active PSs with the inherent biocompatibility of BSA, yielding nanoscale PSs with superior water dispersibility, better biocompatibility and effective PDT to cancer cells.

Based on above description, in this research work, two type BSA encapsulated AIE-active PSs' nanoparticles (NPs) were designed and prepared. First, the incorporation of alkyne group into AIEgens to fabricate two donor (D)-acceptor (A) type PSs (namely as PS-1 and PS-2) by ingenious chemical synthesis. Then, BSA was used to react with above AIE-active PSs to afford AIE-active PSs' NPs via light-mediated thiol-yne click addition reaction (**Scheme 1**). The detail synthetic processes were described in the supporting information (**Figure S1**). For the molecular design, PS-2 had additional electronic acceptor of benzothiadiazole than PS-1, which was expected to achieve red fluorescence of BSA@PS NPs. Experimental result showed that resulting nanocomposites retain the AIE-active PSs' robust ROS generation capability. Systematic evaluations demonstrated that these BSA-based AIE-active PSs' NPs form small

nanoparticles with diameters of near 100 nm. *In vitro* studies further revealed their potent anticancer cells efficacy under light irradiation, achieving over 90% cancer cell ablation, alongside excellent photostability and minimal dark toxicity. This work represents an effective method in fabricating biocompatible AIE-active PS's NPs, which is expected to provide a foundational framework for the industrial-scale production of biocompatible AIE-active PSs.

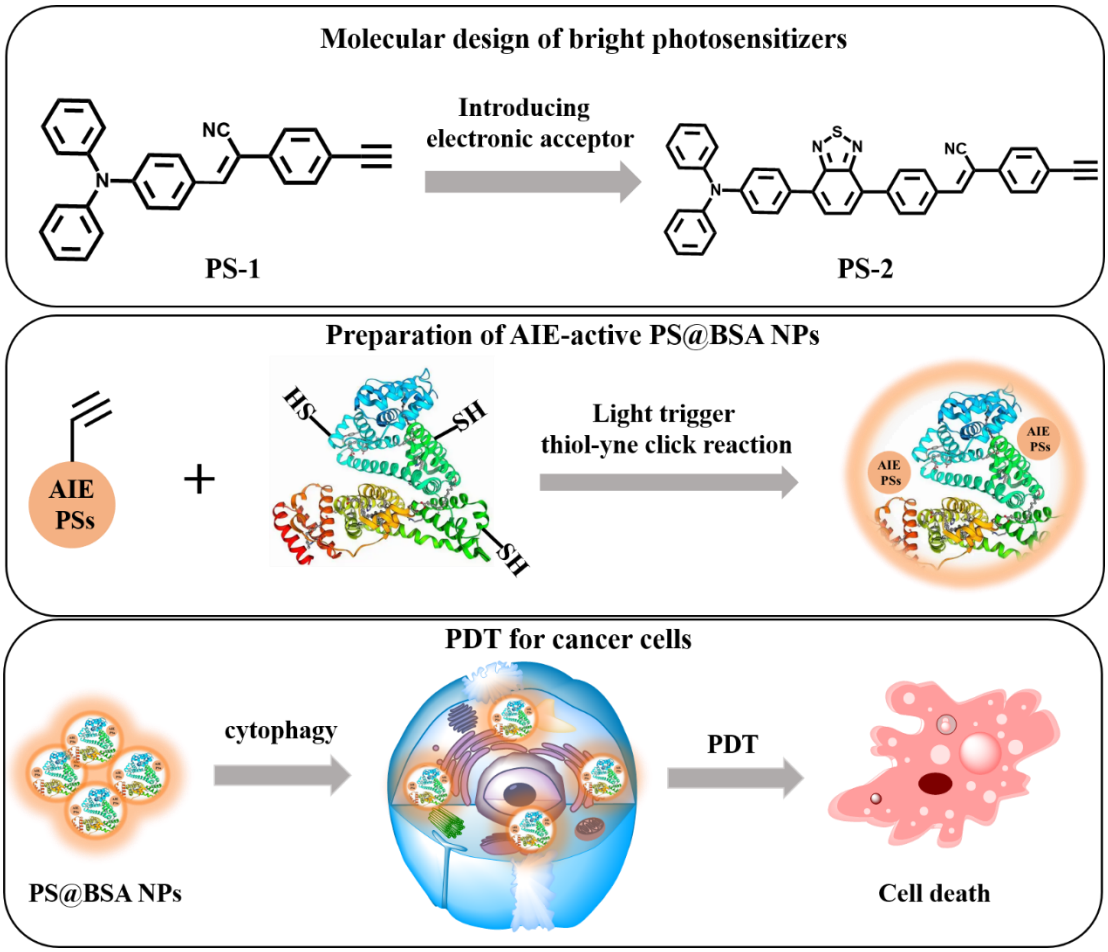

Scheme 1 Demonstration of molecular structures of PSs and light trigger thiol-yne click reaction to fabricate AIE-active PS@BSA nanoparticles for photodynamic anticancer cells.

Results and discussion

Synthesis and characterization of PS-1 and PS-2

Targeted PS-1 and PS-2 were synthesized by combining typical chemical reaction of Suzuki reaction and Knoevenagel condensation reaction, which was purified by the filtration and wash for three times by using heated ethanol with a better yields of 83% and 72%. Firstly, molecular structure of PS-1 was constructed by adopting triphenylamine (TPA) as electronic donor and phenylacetonitrile as electronic acceptor. Differently, PS-2 had additional electronic acceptor of benzothiadiazole than PS-1, which was expected to redshift maximal fluorescence peak.[24] Chemical structures of intermediate and final products were clearly characterized by hydrogen/carbon nuclear magnetic resonance ($^{1}H/^{13}C$ NMR) and high-resolution mass spectra (**Figure S2-8**).

Photophysical properties and theoretical calculation

The photophysical properties of PS-1 and PS-2 were initially evaluated (**Figure 1A**). Both compounds demonstrated good solubility in tetrahydrofuran (THF), with absorption maxima observed at 405 nm and 495 nm, respectively. Their photoluminescence (PL) spectra with maximal emissive wavelength peaked at 557 nm and 629 nm, respectively. Therefore, photophysical property of absorption and fluorescent spectra suggested that PS-1 emitted yellow fluorescence and PS-2 emitted red fluorescence, ascribed to the enhanced intramolecular charge transfer (ICT) effect after inserting electronic acceptor of benzothiadiazole in the PS-2.[25-26] Notably, PS-1 achieved a significantly higher photoluminescence

quantum yield (32.7%) in neat film compared to PS-2 (11.4%), it mightbe contributed to the intramolecular charge transfer (ICT) effect quenched fluorescence.[27] In addition to this reason, different molecular packing modes of these two emitters might cause the difference on their photoluminescence quantum yields.[28-29] Theoretical analyses of frontier molecular orbital distributions revealed electron transition process (**Figure 1B**). For the highest occupied molecular orbital (HOMO) of PS-1, electron density localized predominantly on the triphenylamine unit, while the electron of the lowest unoccupied molecular orbital (LUMO) concentrated at phenylacetonitrile unit. Differently, electrons of HOMO of PS-2 distributed on the units of triphenylamine and benzothiadiazole, while the LUMO's electrons also concentrated at benzothiadiazole and phenylacetonitrile unit. Theoretical calculation of transition decay was carried out, PS-1 and PS-2 had the transition decay of 4.63 Debay and 5.71 Debay, the larger transition decay of PS-2 was well match with its longer absorption and emissive wavelength.

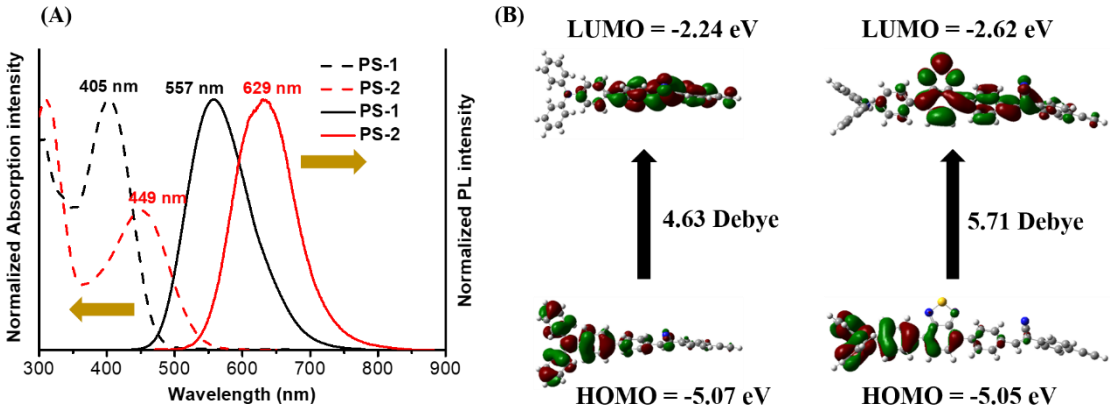

Figure 1 (A) UV-vis absorption andd PL spectra of PS-1 and PS-2 in THF solvent; (B)

Electron distribution of HOMOs/LUMOs and their calculated values based on b3lyp/6-31g(d,p). [PS-1] = 10 μM, [PS-2] = 10 μM.

To explore the correlation between solvent polarity and emitter's fluorescence, ultraviolet visible (UV-vis) absorption and photoluminescence spectra of the two emitters were recorded in different organic solvents with different polarity. Absorption spectra showed small maximal spectral shift accompanying with increased solvent polarity (**Figure 2A-B**), indicating negligible solvatochromic effect of ground-state electronic structure to environmental polarity. Oppositely, excited-state property displayed obvious polarity-dependent trend, evidenced by progressive emission redshift and fluorescence attenuation across the solvent gradient (**Figure 2C-D**). PS-1 exhibited a bathochromic displacement from 493 nm in hexane to 634 nm in dimethyl sulfoxide (DMSO), while PS-2 manifested analogous solvatochromic behavior, shifting from 538 nm to 674 nm under same condition (**Figure 2E-F**). This pronounced excited-state sensitivity stemmed from polar media-induced stabilization of ICT state, as supported by spectral progression trend.[30] The solvent-dependent spectral alterations conclusively validate strong ICT attributes in both emitters, with solvation effects preferentially stabilizing charge-separated excited-state configurations in highly polar environments.

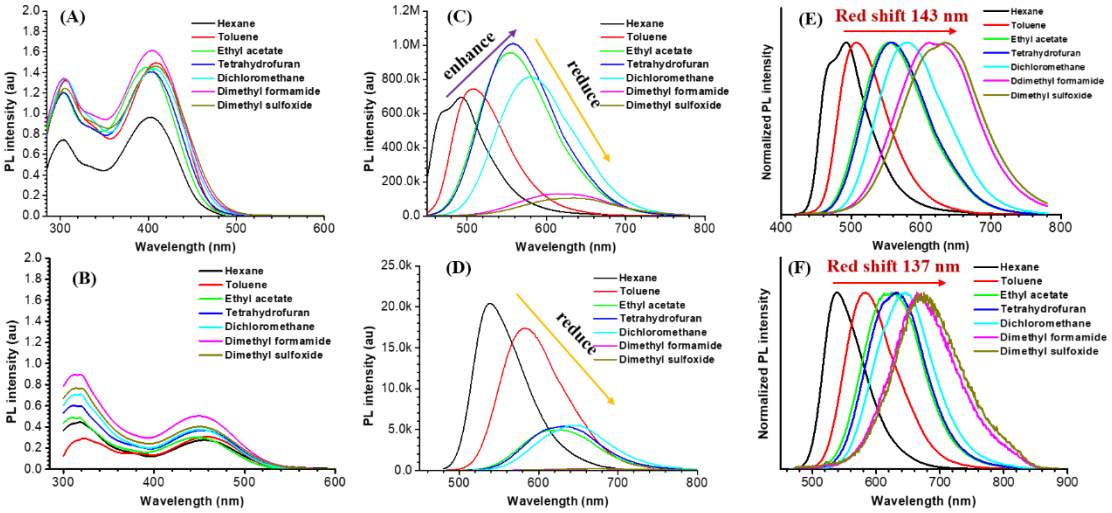

Figure 2 Absorption spectra of PS-1 (A) and PS-2 (B) in different organic solvents; PL spectra of PS-1 (C) and PS-2 (D) in different organic solvents; Normalized PL spectra of PS-1 (E) and PS-2 (F) in different organic solvents. Concentration: 20 μM.

AIE property of both emitters were systematically evaluated. Firstly, the PLQYs of these two emitters in DMSO and neat film were measured. the PLQYs of PS-1 and PS-2 were detected as 22.5% and 18.9% in DMSO. In neat film, the PLQYs of PS-1 and PS-2 were 32.7% and 11.4%, above results suggested preliminarily that PS-1 had aggregation enhanced emission (AEE) nature, but PS-2 might show aggregation caused fluoresence quench effect. To further confirm their AIE property, as depicted in **Figure 3A-B**, their PL spectra displayed distinct emission trends in DMSO/H_2O mixture with incremental aqueous content. In pure DMSO, the emitters exhibited orange fluorescence, contrasting sharply with classical AIE luminogens (AIEgens) like tetraphenylethylene (TPE) and hexaphenylsilole (HPS),[31-32] where dissolved in good solvents typically exhibited very weak fluorescence. For the PS-1, when increasing the water fraction to 60%, fluorescence intensity enhanced progressively

alongside a 76 nm blue shift in maximal emission peak. The improved fluorescent intensity was contributed to the AIE effect, while blue shift of maximal emissive peak within 60% water fraction could be attributed to the changed polar environment from high-polarity DMSO solvent to low-polarity aggregates. Similarly, PS-2 also showed that the fluorescence intensity decreased first and then increased, which was contributed to the synergistic effect of "AIE+TICT".[33]

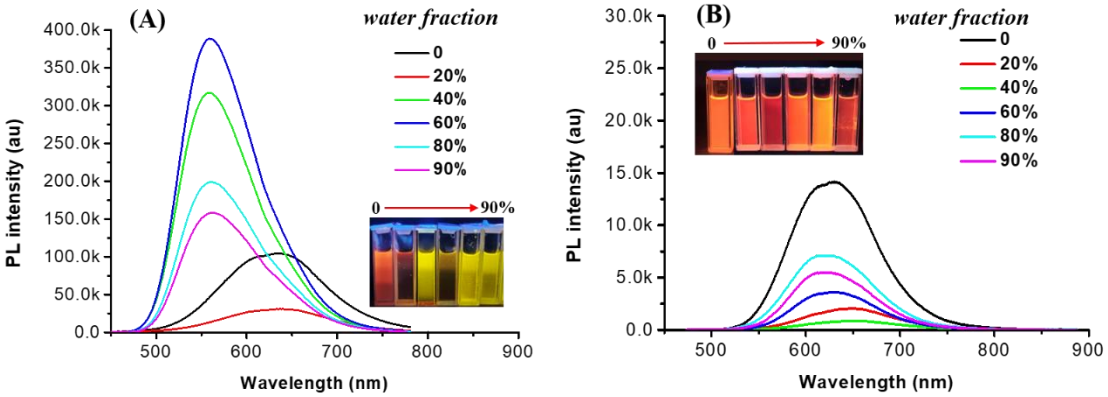

Figure 3 Fluorescent spectra of PS-1 (A) and PS-2 (B) in DMSO/H_2O mixture solvents with different water fraction. Concentration: 20 μM.

Detection of reactive oxygen species

PDT functions as a non-invasive therapeutic approach that leverages light-activated PSs to generate cytotoxic ROS. This mechanism relies on biocompatible PSs absorbing visible light to generate triplet excited states, which then facilitates energy and electron transfer to molecular oxygen. To quantitatively assess ROS production in PS-1 and PS-2, we utilized DCFH dye, a fluorescent probe emitting at maximal 524 nm upon oxidation by ROS. Both PSs demonstrated efficient ROS generation under white light irradiation, consistent with their strong visible-light absorption capability.

Control experiments (**Figure S9A**) revealed minimal background fluorescence from 2',7'-dichlorofluorescein diethylenetriacetate (DCFH-DA) alone under illumination. In contrast, solutions containing PS-1 and PS-2 exhibited substantial fluorescence enhancement upon light exposure (**Figure 4A** and **Figure S9B-C**). Comparative analysis of fluorescent intensity amplification conclusively identified PS-1 as the superior ROS generator under same irradiation condition, achieving markedly higher efficiency than PS-2.

Photodynamic activity generally proceeds through two distinct routes for ROS production: (1) energy transfer from the triplet-excited state of PSs to molecular oxygen, producing singlet oxygen ($^1O_2$), (2) electron transfer reactions that generate superoxide radicals ($O_2^{-\bullet}$) and hydroxyl radicals (•OH).[34] To determine the predominant ROS species generated by PS-1 and PS-2, we utilized the selective $^1O_2$ probe of 9,10-anthracenediyl-bis(methylene)-dimalonic acid (ABDA). The anthracene-based compound ABDA specifically reacts with $^1O_2$ through irreversible endoperoxide formation, enabling quantification via absorbance loss at characteristic wavelengths. Initial control measurement showed negligible absorbance changes in only ABDA solution under prolonged white-light illumination (**Figure 4B** and **Figure S10**). However, systems incorporating PS-1 or PS-2 exhibited marked absorbance reduction, confirming effective $^1O_2$ generation by both PSs. Comparative analysis revealed PS-1 induced

significantly greater ABDA degradation than PS-2, establishing its superior $^1O_2$ production capability under equivalent irradiation conditions.

The generation of type I ROS, specifically $O_2^{-\cdot}$ and ·OH, was systematically investigated using fluorescent probes of dihydrorhodamine 123 (DHR123) and hydroxyphenyl fluorescein (HPF).[35] Initial verification of $O_2^{-\cdot}$ production was conducted through DHR123, a non-fluorescent compound that exhibits distinct green fluorescence emission at 525 nm upon interaction with $O_2^{-\cdot}$. As demonstrated in **Figure 4C** and **Figure S11**, control experiment revealed minimal fluorescence variation in pure DHR123 solutions under 5-minute irradiation. However, significant fluorescence enhancement was observed when PS-1 or PS-2 solution containing DHR123 were exposed to white light, confirming effective $O_2^{-\cdot}$ generation. Subsequent ·OH detection using hydroxyphenyl fluorescein (HPF) probe showed differential radical production between compounds. **Figure 4D** and **Figure S12** illustrated that the PS-2 and HPF combination exhibited stronger fluorescence intensity compared to PS-2 and HPF combination, indicating superior ·OH generation efficiency in PS-2. Therefore, according to above analysis, PS-1 has better $O_2^{-\cdot}$ and $^1O_2$ generation, while PS-2 shows more efficient ·OH generation than PS-1.

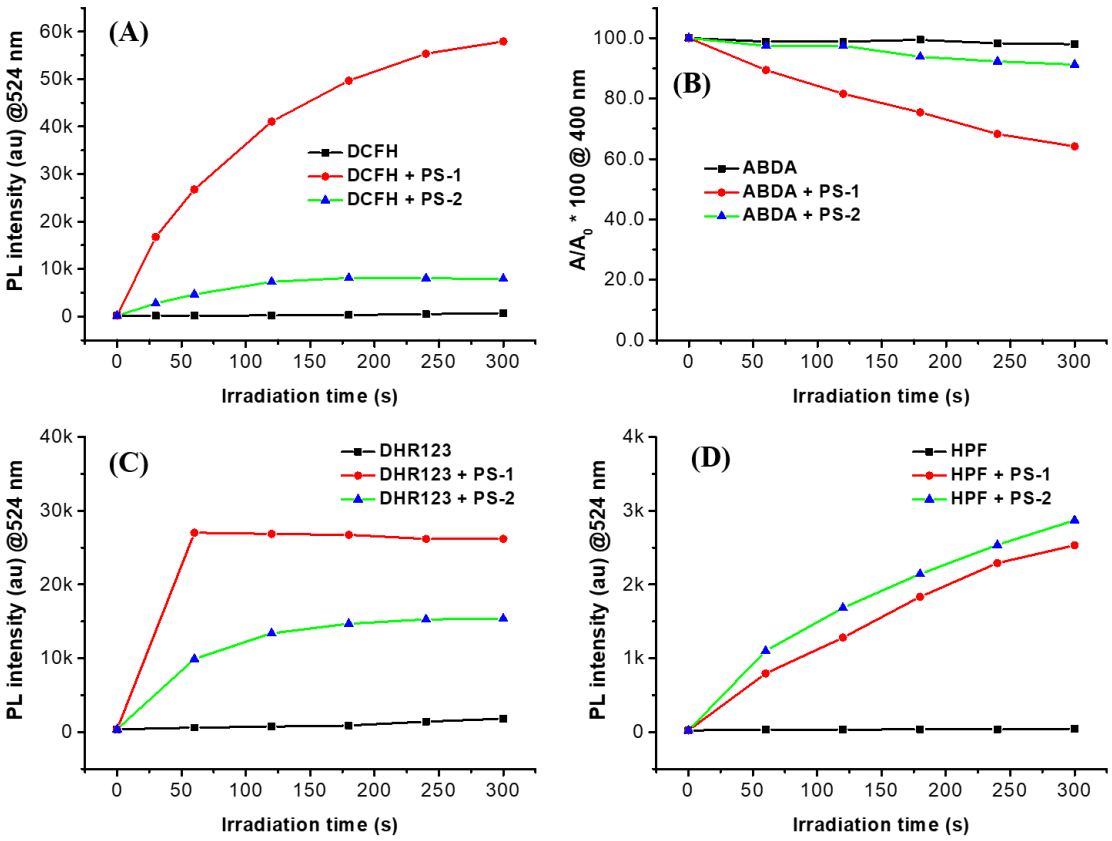

Figure 4. (A) Measurement of total ROS of PS-1 (5 μM) and PS-2 (5 μM) by using DCFH (10 μM) probe upon white light irradiation, (B) access of $^1O_2$ generation with the decomposition of ABDA (20 μM) probe after mixing PS-1 (5 μM) and PS-2 (5 μM) upon white light irradiation, (C) access of $O_2^{\cdot-}$ generation of PS-1 (2 μM) and PS-2 (2 μM) by using DHR123 (10 μM) probe upon white light irradiation, (D) access of •OH generation of PS-1 (2 μM) and PS-2 (2 μM) by using HPF (10 μM) probe upon white light irradiation, white light power: 30 mW/cm^2.

PDT effect of B16-F10 cancer cells

Due to the favorable ROS generation and fluorescence efficiency of PS-1 and PS-2, their PDT potential was assessed at the cellular level by choosing B16-F10 cancer cells as research object. However, both PSs exhibited pronounced hydrophobicity, hindering cellular uptake. To address this limitation, the natural polymer of BSA was employed to link covalently with PSs to enhance their hydrophilia because alkynyl of PSs could happen click reaction with thiol group of BSA, therefore yielding stable PS-

1@BSA NPs and PS-2@BSA NPs with enhanced aqueous dispersibility. Dynamic light scattering (**Figure S13A-B**) revealed hydrodynamic diameters of near 100 nm for PS-1@BSA NPs and PS-2@BSA NPs, with nanoscale dimensions promoting efficient cellular uptake. Their zeta potentials were measured as -36.43 mV and -37.03 mV, and the encapsulation efficiency of PS-1@BSA NPs and PS-2@BSA NPs are about 25.0% and 34.7%. Furthermore, two NPs have better photostability after frequent irradiation by UV light because of not obvious reduction of absorption intensity (**Figure S14**). Next, photophysical properties and ROS performance of PS-1@BSA NPs and PS-2@BSA NPs were characterized. As shown in **Figure S15**, comparing the absorption spectra of PS-1/ PS-1@BSA NPs and PS-2/ PS-2@BSA NPs, it can be known that absorption spectra of BSA-based NPs show a significant redshift phenomenon. For example, PS-1 in THF had the maximal absorption spectrum of 405 nm, but red-shifted to the 434 nm after forming PS-1@BSA NPs. PS-2@BSA NPs showed maximal absorption wavelength of 496 nm, which was larger than PS-2 in THF with maximal absorption peak of 451 nm. Oppositely, comparing with PS-1/PS-2 in THF, the maximal emissive peaks of PS-1@BSA NPs and PS-2@BSA NPs showed a slight blueshift (**Figure S16**). Probes of DHR123 and HPF were used to characterize the type I ROS generation of PS-based BSA NPs, as shown in **Figure S17-18**, fluorescent intensity from DHR123 and HPF showed obvious enhancement,

suggesting an effective generation of $O_2^{-\cdot}$ and •OH.

To evaluate intracellular ROS production, the DCFH fluorescent probe was utilized, B16-F10 cancer cells co-treated with PS@BSA NPs exhibited bright green fluorescence, confirming effective ROS generation (**Figure S19**). According to **Figure 5C-D**, cytocompatibility study demonstrated that over 95% cell viability at high PS@BSA NPs concentration (200 μg/mL), underscoring their better biocompatibility. Upon light irradiation, both PS@BSA NPs caused substantial cell death, validating their great PDT efficacy. Live/dead staining assays further corroborated effective PDT result (**Figure 5E**), that are, when B16-F10 cancer cells uptake PS-1@BSA NPs and PS-2@BSA NPs, after a period of white light irradiation, a large area of cells showed obvious red fluorescence. It was directly proved that the prepared PS-1@BSA NPs and PS-2@BSA NPs had good PDT efficacy, which is expected to show great application potential for treating cancer.

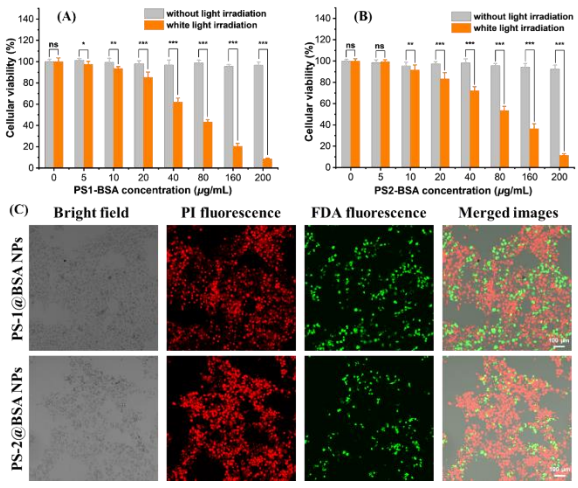

Figure 5 (A) PS-1@BSA NPs, (B) PS-2@BSA NPs against B16-F10 cancer cells at varying concentrations, (C) Live/dead cell costaining assays using FDA and Propidium

iodide (PI) as fluorescence probes for PS-1@BSA NPs and PS-2@BSA NPs, scale bar: 100 μm, [PI] = 2 μM, [FDA] = 5 μM, [PS-1@BSA NPs] = 200 μg/mL, [PS-2@BSA NPs] = 200 μg/mL, white light: 30 mW cm^{-2}.

Conclusion

In summary, this work reported an effective click reaction to fabricate BSA encapsulates the AIE-active PS's NPs. Two alkynyl-contained AIE-active PSs with bright fluorescence and strong generating capability of type I/II ROS at aggregation were designed and synthesized, and their chemical structures were full confirmed by using $^{1}H/^{13}C$ NMR spectra and HRMS spectra. When mixing BSA and PS-1/PS-2 solution and receiving UV light irradiation, two stable PS-1@BSA NPs and PS-2@BSA NPs with enhanced aqueous dispersibility and small size of near 100 nm were obtained, which could effectively produce type I ROS of $O_2^{-\cdot}$ and ·OH, which showed good PDT efficacy to the B16-F10 cancer cells. This work proposed a universal and eco-friendly method for constructing hydrophilic AIE-active PS's NPs, which is expected to show huge promising potential for future biomedical applications.

Conflict of interest statement

There are no conflicts to declare.

Acknowledgements

This work is supported by Special fund for laboratory animals of Gansu Natural Science Foundation (24JRRA379), Foundation of Gansu Province

(23JRRA1518), Provincial Talent Project of Gansu Province (GZTZ2024-4), Project of Gansu Provincial Department of Education (2023QB-056), Talent Innovation and Entrepreneurship Project of Lanzhou City (2022-RC-49), Talent Innovation and Entrepreneurship Project of Chengguan District (2022-rc-7), Scientific Research Fund Project of the Hospital(GMCCH2024-2-4).

References

[1] Pham, T. C.; Nguyen, V.; Choi, Y.; Lee, S.; Yoon, J. Recent Strategies to Develop Innovative Photosensitizers for Enhanced Photodynamic Therapy. Chem. Rev. **2021**, *121*, 13454-13619.

[2] Zhang, W.; Ahmed, A.; Cong, H.; Wang, S.; Shen, Y.; Yu, B. Application of multifunctional BODIPY in photodynamic therapy. Dyes Pigments. **2021**, *185*, 108937.

[3] Algorri, J. F.; Ochoa, M.; Roldán-Varona, P.; Rodríguez-Cobo, L.; López-Higuera, J. M. In Cancers, 2021; Vol. 13.

[4] Tao, T.; Hu, X.; Sun, D.; Ou, C.; Guo, Y.; Xu, H. The halogen effect of bis-truxene substituted BODIPY photosensitizers for potential photodynamic therapy. Dyes Pigments. **2024**, *224*, 111996.

[5] Yu, Y.; Jia, H.; Liu, Y.; Zhang, L.; Feng, G.; Tang, B. Z. Recent Progress in Type I Aggregation-Induced Emission Photosensitizers for Photodynamic Therapy. Molecules, **2023**, *28*, 332.

[6] Ni, J.; Wang, Y.; Zhang, H.; Sun, J. Z.; Tang, B. Z. Aggregation-Induced Generation of Reactive Oxygen Species: Mechanism and Photosensitizer Construction. Molecules, **2021**, *26*, 268.

[7] Wang, X.; Yang, L.; Li, Y. H.; Wang, X. H.; Qi, Z. J. A Long-Retention Cell Membrane-Targeting AIEgen for Boosting Tumor Theranostics. Chem-AsianJ. **2024**, *19*, e202400305.

[8] Wang, X.; Tang, Y. Q.; Liang, J. K.; Zhao, Y. F.; Yang, L.; Qi, Z. J. A lipid droplet-specific near-infrared automatic oxygen-supplied AIEgen for photodynamic therapy and metastasis inhibition of hypoxic tumors. Chem. Eng. J. **2023**, *453*, 139838.

[9] Gao, J.; Tian, Y.; Li, Y.; Hu, F.; Wu, W. Design strategies for aggregation-induced emission photosensitizers with enhanced safety in photodynamic therapy. Coord. Chem. Rev. **2024**, *507*, 215756.

[10] Wan, Q.; Li, Y.; Ding, K.; Xie, Y.; Fan, J.; Tong, J.; Zeng, Z.; Li, Y.; Zhao, C.; Wang, Z.et al. Aggregation Effect on Multiperformance Improvement in Aryl-Armed Phenazine-Based Emitters. J. Am. Chem. Soc. **2023**, *145*, 1607-1616.

[11] Li, Y.; He, D.; Wan, Q.; Tang, B. Z.; Wang, Z. An innovative stepwise activated coupling reaction for fabricating functional fluorescence probes with potential photosensitive applications. Sensor Actuator B-Chem. **2024**, *412*, 135725.

[12] Wang, X.; Li, Y. H.; Hasrat, K.; Yang, L.; Qi, Z. J. Sequence-

Responsive Multifunctional Supramolecular Nanomicelles Act on the Regression of TNBC and Its Lung Metastasis via Synergic Pyroptosis-Mediated Immune Activation. Small, **2023**, *19*, 2305101.

[13] Wang, X.; Li, Y. H.; Qi, Z. J. Light-Enhanced Tandem-Responsive Nano Delivery Platform for Amplified Anti-tumor Efficiency. ChemAsianJ. **2024**, *19*, e202400311.

[14] Zheng, Y.; Li, Y.; Bai, X.; Teng, M.; Tang, Y.; Zhao, S.; Ma, Z.; Liang, H.; Xie, Y.; Wan, Q. Atomic Engineering and Aggregation Effect to Regulate Synergistically Type I Reactive Oxygen Species of AIE-Active Deep Red/Near Infrared Red Photosensitizer. Small **2025**, *21*, 2410816.

[15] Min, X.; Yi, F.; Han, X.; Li, M.; Gao, Q.; Liang, X.; Chen, Z.; Sun, Y.; Liu, Y. Targeted photodynamic therapy using a water-soluble aggregation-Induced emission photosensitizer activated by an acidic tumor microenvironment. Chem. Eng. J. **2022**, *432*, 134327.

[16] Li, X.; Xiong, Y. Application of "Click" Chemistry in Biomedical Hydrogels. ACS Omega **2022**, *7*, 36918-36928.

[17] Kaur, J.; Saxena, M.; Rishi, N. An Overview of Recent Advances in Biomedical Applications of Click Chemistry. Bioconjug. Chem. **2021**, *32*, 1455-1471.

[18] Albada, B.; Keijzer, J. F.; Zuilhof, H.; van Delft, F. Oxidation-Induced "One-Pot" Click Chemistry. Chem. Rev. **2021**, *121*, 7032-7058.

[19] McDaniel, R. M.; Carey, M. S.; Wilson, O. R.; Barsoum, M. W.;

Magenau, A. J. D. Well-Dispersed Nanocomposites Using Covalently Modified, Multilayer, 2D Titanium Carbide (MXene) and In-Situ “Click” Polymerization. Chem. Mat. **2021**, *33*, 1648-1656.

[20] Sradha S, A.; Sariga; George, L.; Varghese, A. Advancements in thiol-yne click chemistry: Recent trends and applications in polymer synthesis and functionalization. Mater. Today Chem. **2024**, *38*, 102112.

[21] Lü, S.; Wang, Z.; Zhu, S. Thiol-Yne click chemistry of acetylene-enabled macrocyclization. Nat. Commun. **2022**, *13*, 5001.

[22] Wang, B.; Li, C.; He, D.; Ding, K.; Tian, Q.; Feng, G.; Qin, A.; Tang, B. Z. Bioconjugation and Reaction-Induced Tumor Therapy via Alkynamide-Based Thiol-Yne Click Reaction. Small **2024**, *20*, 2307309.

[23] Mitmoen, M.; Kedem, O. UV- and Visible-Light Photopatterning of Molecular Gradients Using the Thiol–yne Click Reaction. ACS Appl. Mater. Interfaces **2022**, *14*, 32696-32705.

[24] Deng, D.; Yang, Y.; Liu, S.; Deng, X.; Chen, Z.; Pu, S. Benzothiadiazole-based dibenzobenzimidazole derivatives with aggregation-induced deep-red fluorescence and different mechanically responsive fluorescence features. Dyes Pigments. **2022**, *205*, 110580.

[25] He, Y.; Xie, F.; Li, H.; Zhang, K.; Shen, Y.; Ding, F.; Wang, C.; Li, Y.; Tang, J. Red-shift emission and rapid up-conversion of B,N-containing electroluminescent materials via tuning intramolecular charge transfer. Mater. Chem. Front. **2023**, *7*, 2454-2463.

[26] Long, J.; Shan, J.; Zhao, Y.; Ji, Y.; Tan, H.; Wang, H. Dramatically Enhanced and Red-shifted Photoluminescence Achieved by Introducing an Electron-withdrawing Group into a Non-traditional Luminescent Small Organic Compound. Chem-Asian J. **2021**, *16*, 2426-2430.

[27] Wu, H.; Du, L.; Luo, J.; Wang, Z.; Phillips, D. L.; Qin, A.; Tang, B. Z. Structural modification on tetraphenylpyrazine: from polarity enhanced emission to polarity quenching emission and its intramolecular charge transfer mechanism. J. Mater. Chem. C **2022**, *10*, 8174-8180.

[28] Wang, J. F.; Cao, M. Y.; Han, L. L.; Shangguan, P.; Liu, Y. S.; Zhong, Y.; Chen, C. Y.; Wang, G. Y.; Chen, X. Y.; Lin, M.; Lu, M. Y.; Luo, Z. Q.; He, M.; Sung, H. H. Y.; Niu, G. L.; Lam, J. W. Y.; Shi, B. Y.; Tang, B. Z. Blood–Brain Barrier-Penetrative Fluorescent Anticancer Agents Triggering Paraptosis and Ferroptosis for Glioblastoma Therapy, J. Am. Chem. Soc. **2024**, *146*, 42, 28783–28794.

[29] Cao, S. X.; Tian, X. Y.; Cao, M. Y.; Wang, J. G.; Niu, G. L.; Tang, B. Z. Solvatochromic Near-Infrared Aggregation-Induced Emission-Active Acrylonitriles by Acceptor Modulation for Low-Power Stimulated Emission Depletion Nanoscopy, Chem. Mater. **2023**, *35*, 6, 2472–2485.

[30] Wan, Q.; Dai, W.; Xie, Y.; Ke, Q.; Zhao, C.; Zhang, B.; Zeng, Z.; Wang, Z.; Tang, B. Z. AIE-active deep red/near-infrared electroluminescent emitters with fine regulation of excited state. Chem. Eng. J. **2023**, *451*, 138529.

[31] Li, D.; Zuo, R.; Wang, J.; Le, Z. The Designs and Applications of Tetraphenylethylene Macrocycles and Cages. Chem-Eur J. **2025**, *31*, e202403715.

[32] Ito, F. Fluorescence Detection of Dynamic Aggregation Processes Using AIEgens, 2022.

[33] Huang, J.; Zhou, Y.; Wang, W.; Zhu, J.; Li, X.; Fang, M.; Wu, Z.; Zhu, W.; Li, C. A fluorescent probe based on triphenylamine with AIE and ICT characteristics for hydrazine detection. Spectrochimica Acta Part a: Molecular and Biomolecular Spectroscopy **2023**, *286*, 122011.

[34] Tang, Y.; Xie, Y.; Bai, X.; Zhao, C.; Zheng, Y.; Liang, H.; Ma, Z.; Wang, Z.; Wan, Q. Building Block for Designing Bright Type I AIE-Active Photosensitizers with Deep/Near-infrared Red Fluorescence. Chemistry – an Asian Journal **2025**, *20*, e202401276.

[35] Wan, Q.; Zhang, R.; Zhuang, Z.; Li, Y.; Huang, Y.; Wang, Z.; Zhang, W.; Hou, J.; Tang, B. Z. Molecular Engineering to Boost AIE-Active Free Radical Photogenerators and Enable High-Performance Photodynamic Therapy under Hypoxia. Adv. Funct. Mater. **2020**, *30*, 2002057.

Graphical Abstract

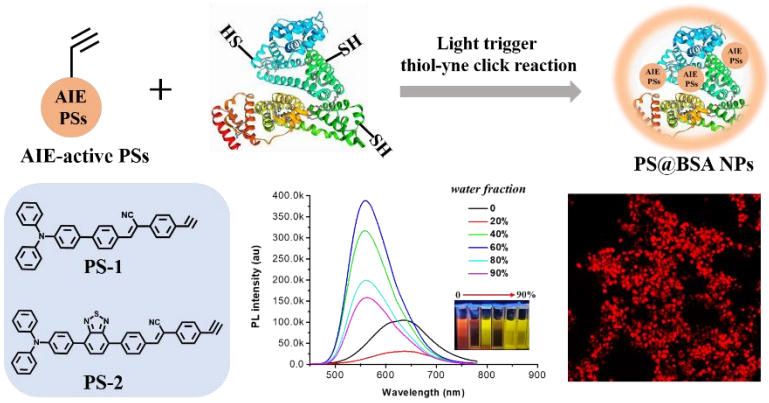

This work proposed a universal and eco-friendly light trigger thiol-yne click reaction method for preparing hydrophilic AIE-active photosensitizer's nanoparticles, which achieved great photodynamic therapy effect for the B16-F10 cancer cells.

Declaration of interests

☒ The authors declare that they have no known competing financial interests or personal relationships that could have appeared to influence the work reported in this paper.

☐The authors declare the following financial interests/personal relationships which may be considered as potential competing interests: